Involvement of receptor for advanced glycation end products in microgravity-induced skeletal muscle atrophy in mice

Tatsuro Egawa[1], Kohei Kido[2], Takumi Yokokawa[2,3], Mami Fujibayashi[4], Katsumasa Goto[5], Tatsuya Hayashi[2]

[1] Laboratory of Health and Exercise Sciences, Graduate School of Human and Environmental Studies, Kyoto University, Kyoto, Japan.
[2] Laboratory of Sports and Exercise Medicine, Graduate School of Human and Environmental Studies, Kyoto University, Kyoto, Japan.
[3] Research Organization of Science and Technology, Ritsumeikan University, Shiga, Japan.
[4] Division of Physical and Health Education, Setsunan University, Osaka, Japan.
[5] Laboratory of Physiology, Graduate School of Health Sciences, Toyohashi SOZO University, Aichi, Japan.

Address for correspondence:
Tatsuro Egawa, Ph.D.
Laboratory of Health and Exercise Sciences, Graduate School of Human and Environmental Studies, Kyoto University, Yoshida-nihonmatsu-cho, Sakyo-ku, Kyoto 606-8501, Japan.
Telephone +81-75-753-6613, Fax: +81-75-753-6885
E-mail: egawa.tatsuro.4u@kyoto-u.ac.jp

List of abbreviations

AGEs: advanced glycation end-products

AGE-R1: AGE receptor 1

ALDH: aldehyde dehydrogenase

CBB: Coomassie Brilliant Blue

CML: Nε-(carboxymethyl) lysine

CSA: cross sectional area

IL: interleukin

LC3: microtubule-associated protein 1 light chain 3

MG: methylglyoxal

MyHC: myosin heavy chain

MuRF1: muscle RING finger protein 1

p70S6K: 70-kDa ribosomal S6 kinase

RAGE: receptor for AGEs

TNFα: tumor necrosis factor α

Ulk1: Unc-51-like kinase 1

WWP1: WW domain containing E3 ubiquitin protein ligase 1

Abstract

The accumulation of advanced glycation end-products (AGEs) may be involved in the mechanism of skeletal muscle atrophy. However, the involvement of the receptor for AGEs (RAGE) axis in microgravity-induced skeletal muscle atrophy has not been investigated. Therefore, the purpose of the present study was to investigate the effect of RAGE inhibition on microgravity-induced skeletal muscle atrophy and the related molecular responses. Male C57BL/6NCr mice subjected to a 1-week hindlimb suspension lead to muscle atrophy in soleus and plantaris but not extensor digitorum longus muscle, accompanied by increases in RAGE expression. However, treatment with a RAGE antagonist (FPS-ZM1, intraperitoneal, 1 mg/kg/day) during hindlimb suspension ameliorated the atrophic responses in soleus muscle. Further, muscle mass inversely correlated with the accumulation of AGEs (methylglyoxal-modified proteins and Nε-(carboxymethyl) lysine-modified proteins) in soleus muscle. The expression of proinflammatory cytokines, tumor necrosis factor-α, interleukin-1β, and interleukin-6 in soleus muscle was enhanced in response to hindlimb suspension, but these changes were attenuated by FPS-ZM1 treatment. Protein ubiquitination and ubiquitin E3 ligase (muscle RING finger 1) expression in soleus muscle were elevated following hindlimb suspension, and these increments were suppressed by FPS-ZM1 treatment. Our findings indicate that the AGE-RAGE axis is upregulated in unloaded atrophied skeletal muscle, and that RAGE inhibition ameliorates microgravity-induced skeletal muscle atrophy by reducing proinflammatory cytokine expression and ubiquitin-proteasome system activation.

Keywords: RAGE, interleukin-1, interleukin-6, methylglyoxal, tumor necrosis factor-α, ubiquitin-proteasome system

1. Introduction

Skeletal muscle mass is regulated by the balance between protein synthesis and degradation, which increase and reduce it, respectively. Skeletal muscle atrophy can be caused by several physiological and pathological conditions, such as unloading, aging, malnutrition, burns, diabetes, cancer cachexia, sepsis, chronic renal failure, and chronic obstructive pulmonary disease [1]. In particular, exposure to microgravity environments has been well reported to result in marked skeletal muscle atrophy accompanied by the changes of morphological, metabolic, and contractile properties [2].

Recently, glycation can been shown to be involved in the mechanism of skeletal muscle atrophy [3, 4]. Glycation is non-enzymatic reaction between reducing sugars or aldehydes with proteins, DNA, or lipids, resulting in the formation of glycation adducts and advanced glycation end-products (AGEs). Glycation results in cell and tissue damage by inhibiting the biological functions of proteins and activating the AGE receptor (receptor for advanced glycation end-products, RAGE) [5]. Epidemiological studies have shown that AGE accumulation is associated with low skeletal muscle quality [6, 7]. In addition, experimental studies have demonstrated that the treatment of cultured muscle cells with AGEs induces muscle atrophy [3, 8] and that long-term consumption of an AGE-containing diet results in the accumulation of AGEs in skeletal muscle and muscle dysfunction [9].

AGEs stimulate several signaling pathways *via* a series of cell surface receptors, the most studied of which is RAGE, a multi-ligand member of the immunoglobulin superfamily. The involvement of the AGE-RAGE axis in several diseases, including diabetic complications, cardiovascular disease, Alzheimer's disease, and osteoporosis is well established [10]. In this context, a variety of RAGE antagonists are now available for preclinical and clinical studies [11, 12]. For example, TTP488 (azeliragon), which is an orally-active small-molecule antagonist of RAGE, improves cognitive function in Alzheimer disease patients by inhibiting inflammation and amyloid-β accumulation [13]. FPS-ZM1, which was identified by screening 5,000 compounds for their ability to inhibit RAGE and amyloid-β interaction, can block amyloid-β-induced cellular stress in RAGE-expressing brain endothelium, neurons, and microglia [14].

It has been shown that AGEs induce muscle atrophy *via* RAGE-mediated signaling in cultured muscle cells [3] and that AGE-induced impairment in insulin signaling is

mediated by RAGE in cultured muscle cells and rats [15]. Furthermore, a recent study has shown that pharmacological inhibition of RAGE ameliorates the aging-induced loss of muscle mass in middle-aged mice [16]. These evidences suggest that inhibition of the AGE-RAGE axis may be an effective means of treating skeletal muscle atrophy under conditions in which the AGE-RAGE axis is activated. However, it has not been investigated whether the AGE-RAGE axis is activated on microgravity environment, or whether inhibition of the AGE-RAGE axis ameliorates microgravity-induced skeletal muscle atrophy and the related molecular responses. In the present study, therefore, we investigated the involvement of AGE-RAGE axis, by using the RAGE antagonist, FPS-ZM1, in skeletal muscle atrophy following hindlimb suspension, which is a well-established approach to create a ground-based model of microgravity.

2. Materials and Methods

2.1. Animals

Male 10-week-old C57BL/6NCr mice were purchased from Shimizu Breeding Laboratories (Kyoto, Japan), housed in a room maintained at 22–24°C, under a 12:12 h light/dark cycle, and fed a standard laboratory diet and water *ad libitum*. All animal procedures were carried out in accordance with the Guide for the Care and Use of Laboratory Animals published by the National Institutes of Health (Bethesda, MD, USA) and were approved by the Kyoto University Graduate School of Human and Environmental Studies (approval number: 28-A-2).

2.2. Hindlimb suspension procedure

Experiment 1: Mice were divided into two groups: a control (n = 8) and a hindlimb suspension (HS, n = 6) group. The HS group was subjected to continuous hindlimb suspension for 1 week, as described previously [17]. After the experimental period, soleus, plantaris, and extensor digitorum longus (EDL) muscles were dissected from each mouse under anesthesia and used for western blotting. Blood samples were collected from a carotid artery into tubes containing heparin as an anticoagulant, and plasma was separated by centrifugation at 8,000 × *g* for 15 min and used for the measurement of fluorescence intensity, corresponding to AGE concentration. Age-matched animals that did not undergo hindlimb suspension were used as controls. The fluorescence intensity corresponding to AGE concentration was measured using 360 nm excitation and 460 nm emission wavelengths on a Synergy LX Multi-Mode Microplate Reader (BioTek, Winooski, VT, USA). The intensity levels were normalized to protein content and are expressed in arbitrary units.

Experiment 2: Mice were divided into three groups: a control group (n = 16), a hindlimb suspension group (n = 18), and a hindlimb suspension +FPS-ZM1 group (n = 16). Mice in the HS group were subjected to continuous hindlimb suspension for 1 week. Mice in the hindlimb suspension +FPS-ZM1 group were injected daily intraperitoneally with 1 mg/kg FPS-ZM1 (Millipore, Burlington, MA, USA) during the hindlimb suspension procedure, and the mice in the hindlimb suspension group were injected daily the equal volume of saline as a treatment control. The dose of FPS-ZM1 used was as previously published [18]. After the experimental period, soleus muscles were dissected

from each mouse under anesthesia and weighed. A separate set of right muscle (n = 8-10/group) and left muscle (n = 8-10/group) were frozen in liquid nitrogen and used for western blotting and real-time RT-PCR analysis, respectively. Another separate set of right muscle (n = 8/group) was immediately frozen in 2-methylbutane cooled with liquid nitrogen and used for muscle fiber cross-sectional area (CSA) analysis. Age-matched animals that did not undergo hindlimb suspension were used as controls.

2.3. Sample preparation and western blotting

Sample preparation and western blot analysis were performed as described previously [19]. Muscles were homogenized in ice-cold lysis buffer (1:40 w/v) containing 20 mM Tris-HCl (pH 7.4), 1% Triton-X, 50 mM NaCl, 250 mM sucrose, 50 mM NaF, 5 mM sodium pyrophosphate, 2 mM dithiothreitol, 4 mg/L leupeptin, 50 mg/L trypsin inhibitor, 0.1 mM benzamidine, and 0.5 mM phenylmethylsulfonyl fluoride, then the homogenates were centrifuged at 16,000 × *g* for 30 min at 4°C, and the supernatants were collected.

The samples were separated by SDS-PAGE using 4–15% polyacrylamide gels, then proteins were transferred to polyvinylidene fluoride membranes (Bio-Rad Laboratories. Hercules, CA, USA). Next, the membranes were blocked for 1 h using Western BLoT Blocking Buffer (Takara Bio, Otsu, Japan) and incubated overnight at 4°C with primary antibodies: RAGE (sc-365154, Santa Cruz Biotechnology, Santa Cruz, CA, USA), MyHC slow-type (sc-32733, Santa Cruz Biotechnology), MG-modified protein (MMG-030n, JaICA, Shizuoka, Japan), Nε-(carboxymethyl) lysine (KH001, Trans Genic, Kobe, Japan), AGE-R1 (sc-74408, Santa Cruz Biotechnology), glyoxalase 1 (GTX628890, Gene Tex, Darmstadt, Irvine, CA), aldose reductase (sc-166918, Santa Cruz Biotechnology), ALDH2 (sc-100496, Santa Cruz Biotechnology), TNFα (sc-52746, Santa Cruz Biotechnology), IL-1β (sc-52012, Santa Cruz Biotechnology), IL-6 (sc-57315, Santa Cruz Biotechnology), K48-linkage specific polyubiquitin (4298, Cell Signaling Technology, Danvers, MA, USA), MuRF1 (sc-398608, Santa Cruz Biotechnology), Ulk1 (8054, Cell Signaling Technology), phospho-Ulk1 Ser^{757} (6888, Cell Signaling Technology), LC3 (2775, Cell Signaling Technology), p62 (5114, Cell Signaling Technology), p70S6K (9202, Cell Signaling Technology), or phospho-p70S6K Thr^{389} (9234, Cell Signaling Technology). The membranes were then washed with Tris-buffered saline containing 0.1% Tween 20 (TBS-T, pH 7.5) and incubated with corresponding

secondary antibodies for 1 h at room temperature. After a final wash with TBS-T, protein bands were visualized using ECL Select (GE Healthcare, Buckinghamshire, UK) and a bioimaging analyzer (LuminoGraph II, ATTO, Tokyo, Japan). The relative band intensities were quantified and normalized to total protein by staining membranes with Coomassie Brilliant Blue (CBB). Phosphorylation level was expressed as the ratio of the phosphorylated form to the total form. For the quantification of MG-modified protein, CML-modified protein, and K48-ubiquitinated protein, the signal intensity of full-molecular-weight was quantified.

2.4. Real-time RT-PCR analysis

Real-time RT-PCR analysis were performed as described previously [9]. Total RNA was extracted from frozen muscles using the RNeasy Mini Kit (Qiagen, Venlo, Netherlands). RNA was reverse-transcribed into cDNA using PrimeScript RT Master Mix (Perfect Real Time, Takara Bio). The synthesized cDNA was subjected to real-time RT-PCR (Step One Real Time System, Applied Biosystems, Carlsbad, CA, USA) using SYBR Premix Ex Taq (Takara Bio) and then analyzed using StepOne Software v2.3 (Applied Biosystems). The relative fold- difference in expression was calculated using the comparative CT method. Ribosomal protein S18 (Rps18) was used as a reference gene. The primers used were as follows: Trim63, 5'-AGGACTCCTGCAGAGTGACCAA-3' (forward) and 5'-TTCTCGTCCAGGATGGCGTA-3' (reverse); Fbxo32, 5'-TGTCCTTGAATTCAGCAAGCAAAC-3' (forward) and 5'-TGTGGCCATCCATTATTTCCAG-3' (reverse); Wwp1, 5'-GACATGGCCACTGCTTCAC-3' (forward) and 5'-GGAGGTCAATTAACGGCTCTG-3' (reverse); and Rps18, 5'-TTGGTGAGGTCAATGTCTGCTTT-3' (forward) and 5'-AAGTTTCAGCACATCCTGCGAGT-3' (reverse).

2.5. Muscle fiber CSA analysis

To measure the CSA of individual fibers, muscle cryostat sections were stained for laminin by the standard immunohistochemical technique [20]. Briefly, frozen serial sections (7 μm) were cut from the midbelly of soleus muscles at -20°C and mounted on glass slides. Cross sections were fixed with 4% paraformaldehyde for 15 min, and then

were post-fixed in ice-cold methanol for 15 min. Sections were blocked for 30 min by using Blocking One Histo (Nacalai tesque, Kyoto, Japan). Then, samples were incubated with the primary antibodies for rabbit polyclonal anti-laminin (L9393, Sigma, St. Louis, MO, USA) overnight at 4°C. Sections were then incubated with the second antibodies for Alexa Fluor 488-conjugated anti-rabbit IgG (Jackson Immunoresearch, West Grove, PA, USA) for 1 h at room temperature. A cover glass was then placed above the section covering Vector Shield (Vector Laboratories, Burlingame, CA, USA). Fiber CSA (~150 fibers/muscle) was automatically measured as the internal laminin-unstained area by using ImageJ.

2.6. Statistical analysis

Data are expressed as means ± SE. Differences between two groups were analyzed using Student's *t*-test. Multiple means were analyzed using the parametric Tukey–Kramer or non-parametric Steel–Dwass multiple comparisons tests, as appropriate. The interrelationships between the relative muscle mass and the levels of AGEs were assessed using Pearson's correlation. Values were considered statistically significant when $P < 0.05$. Effect size was classified using Cohen's r (r = 0.10, small; 0.30, medium; 0.50, large). Effect size is a quantitative measure of the magnitude for the difference between two means and is useful for interpreting biological significance of results rather than just their statistical significance, and further contributes to compare effects across studies (e.g. meta-analytic study) and animal welfare because this index is often used when determining sample size in a planning study [21]. All statistical analyses were performed using Ekuseru-Toukei 2012 software (Social Survey Research Information, Tokyo, Japan).

3. Results

3.1. The AGE-RAGE axis is activated in atrophied muscle by hindlimb suspension

To investigate whether the AGE-RAGE axis is activated by hindlimb suspension, we evaluated the fluorescence intensity of AGEs in plasma and the RAGE expression in soleus, plantaris, and EDL muscle after hindlimb suspension. Several AGEs demonstrate characteristic fluorescence, and therefore the fluorescence intensity is a measure of the accumulation of AGEs [22]. After 1-week hindlimb suspension, the fluorescence intensity of the plasma was significantly elevated (Figure 1A). Both soleus (CON, 0.33 ± 0.01; HS, 0.28 ± 0.01 mg/g, $P = 0.001$, $r = 0.75$), and plantaris (CON, 0.63 ± 0.01; HS, 0.56 ± 0.01 mg/g, $P < 0.001$, $r = 0.78$) mass normalize to body mass were significantly reduced by hindlimb suspension, but not EDL (CON, 0.40 ± 0.01; HS, 0.41 ± 0.01 mg/g, $P = 0.43$, $r = 0.21$). Consistent with this muscle atrophic response, RAGE expression was elevated in soleus and plantaris muscle but not EDL muscle in response to hindlimb suspension (Figure 1B).

3.2. RAGE inhibition ameliorates soleus muscle atrophy induced by hindlimb suspension

To determine whether RAGE inhibition ameliorates skeletal muscle atrophy, we investigated the effect of treatment with the RAGE antagonist, FPS-ZM1, on soleus muscle mass, muscle fiber CSA, and the expression of slow-type myosin heavy chain (MyHC), because skeletal muscle atrophy preferentially affects specific fiber types, and is generally accompanied by a slow-to-fast shift in fiber type and MyHC isoform phenotype during unloading-induced skeletal muscle atrophy [23]. Following hindlimb suspension for 1 week, the ratio of soleus to body mass was significantly lower, but FPS-ZM1 treatment significantly ameliorated this reduction (Figure 2A). Correspondingly, FPS-ZM1 treatment partly cancelled the reduction of muscle fiber CSA (Figure 2B). Further, the expression of slow-type MyHC was significantly downregulated by hindlimb suspension, but FPS-ZM1 treatment tended to ameliorate this reduction with a large effect size (Figure 2C).

3.3. RAGE inhibition suppresses AGE accumulation in soleus muscle induced by hindlimb suspension

To determine the effect of RAGE inhibition on AGE accumulation in atrophied soleus muscle, we measured the levels of methylglyoxal (MG)-modified proteins and Nε-(carboxymethyl) lysine (CML)-modified proteins following hindlimb suspension. MG-derived AGEs and CML-derived AGEs are major glycated proteins found in tissues and are ligands for RAGE [24, 25]. After 1-week hindlimb suspension, MG-modified proteins and CML-modified proteins had accumulated in soleus muscle, but FPS-ZM1 treatment significantly suppressed the accumulation of MG-modified proteinsand tended to ameliorate the accumulation of CML-modified proteins with a middle effect size (Figure 3A). Furthermore, the muscle levels of MG-modified proteins and CML-modified proteins inversely correlated with soleus muscle mass (Figure 3B).

3.4. RAGE inhibition ameliorates the changes in expression of molecules regulating AGE accumulation in soleus muscle induced by hindlimb suspension

To determine the effect of hindlimb suspension and RAGE inhibition on glycation-defense systems, we measured the expression of AGE receptor 1 (AGE-R1), glyoxalase 1, aldose reductase, and aldehyde dehydrogenase (ALDH) 2 following hindlimb suspension (Figure 4). AGE-R1, which is an integral plasma membrane protein, is involved in the detoxification and clearance of AGEs [26], and glyoxalase 1, aldose reductase, and ALDH are enzymes that contribute to the inhibition of AGE formation [27]. After 1-week hindlimb suspension, the expression of AGE-R1, glyoxalase 1, aldose reductase, and ALDH2 was significantly higher, but FPS-ZM1 treatment tended to ameliorate this effect with a large effect size (Figure 4).

3.5. RAGE inhibition ameliorates the inflammatory response induced in soleus muscle by hindlimb suspension

To determine the effects of RAGE inhibition on the inflammatory response, we measured the expression of the proinflammatory cytokines tumor necrosis factor α (TNFα), interleukin (IL)-1β, and IL-6 (Figure 5). While IL-1β exists as a pro-IL-1β and mature-IL-1β, we measured mature-IL-1β because mature form is only active [28]. The expression of TNFα, IL-1β, and IL-6 was significantly increased by 1-week hindlimb suspension, but FPS-ZM1 treatment significantly ameliorated the increase in expression of TNFα, and tended to ameliorate the increases in IL-1β and IL-6 expression with a

middle effect size (Figure 5).

3.6. RAGE inhibition ameliorates the activation of the ubiquitin-proteasome system induced in soleus muscle by hindlimb suspension

To determine the effects of RAGE inhibition on the ubiquitin-proteasome system, we measured the expression of ubiquitin E3 ligases and the levels of K48-ubiquitinated proteins. After the 1-week hindlimb suspension period, muscle RING finger protein 1 (MuRF1) mRNA (*Trim 63*) (Figure 6A) and MuRF1 protein (Figure 6B) were significantly upregulated, but FPS-ZM1 treatment significantly ameliorated these effects. On the other hand, hindlimb suspension had no impact on the expression of atrogin-1 mRNA (*Fbox32*) and WW domain containing E3 ubiquitin protein ligase 1 (WWP1) mRNA (*Wwp1*) (Figure 6A). The levels of K48 ubiquitinated proteins were significantly higher after hindlimb suspension, but FPS-ZM1 treatment tended to ameliorate this effect with a middle effect size (Figure 6B).

3.7. RAGE inhibition does not affect autophagy or the protein synthesis pathway in soleus muscle following hindlimb suspension

To determine the effects of RAGE inhibition on autophagy and protein synthesis pathways, we measured the levels of phosphorylation of Unc-51-like kinase 1 (Ulk1) Ser^{757}, the microtubule-associated protein 1 light chain 3 (LC3) II-to-LC3I ratio, p62 expression, and the phosphorylation of 70-kDa ribosomal S6 kinase (p70S6K) at Thr^{389} following hindlimb suspension (Figure 7). Ulk1 Ser^{757} dephosphorylation, high LC3II-to-LC3I ratio, and p62 breakdown are widely used as markers of autophagy and p70S6K phosphorylation is the primary means of assessing the activity of the protein synthesis pathway. After 1-week hindlimb suspension, the phosphorylation level of Ulk1 Ser^{757}, p62 expression, and the phosphorylation level of p70S6K Thr^{389} were significantly lower, and the LC3II-to-LC3I ratio was significantly higher. However, FPS-ZM1 treatment did not ameliorate these effects (Figure 7).

4. Discussion

We have made several novel findings in the present study regarding the involvement of the AGE-RAGE axis in microgravity-induced skeletal muscle atrophy. First, 1-week hindlimb suspension increased AGE levels and RAGE expression in atrophied soleus and plantaris but not non-atrophied EDL muscle (Figure 1 and 3) or/and the circulation (Figure 1). Second, RAGE inhibition ameliorated the soleus muscle atrophy caused by hindlimb suspension (Figure 2) and proportionately reduced AGE accumulations (Figure 3). Third, hindlimb suspension increased the expression of receptors and enzymes regulating AGE accumulation, and RAGE inhibition reduced these changes (Figure 4). Fourth, RAGE inhibition reduced the upregulation of proinflammatory cytokine expression (Figure 5) and the activation of the ubiquitin-proteasome system (Figure 6) in response to hindlimb suspension. Finally, RAGE inhibition had no effect on the hindlimb suspension-induced activation of autophagy and suppression of the protein synthesis pathway (Figure 7).

AGEs accumulate in the human body with aging, including in the blood, lenses, skin, aorta, liver, bone, brains, tendons, and skeletal muscles [29]. In the past decade, many researchers have shown an inverse relationship between AGE accumulation in the blood or skin and muscle mass and function in elderly people [6, 7]. The intracellular accumulation of AGEs in skeletal muscle has also been shown in aged rats [30, 31]. Another study showed that treatment with alagebrium chloride, an AGE inhibitor, ameliorated skeletal muscle atrophy in diabetic mice [3]. Following that report, our previous studies also demonstrated that long-term AGE loading inhibits skeletal muscle growth and the development of muscle functions, including tension and fatigue resistance, by impairing myogenic capacity and cellular signal transduction [8, 9]. Taken together, these findings suggest that AGE accumulation in the body is a cause of age- or diabetes-induced skeletal muscle dysfunction. In the present study, we found that AGE accumulation occurs in response to hindlimb suspension in only atrophied muscle (Figure 1 and 3) and correlates with muscle mass (Figure 3). Therefore, AGE accumulation may be involved in microgravity-induced skeletal muscle atrophy.

Skeletal muscle possesses a series of defense mechanisms against glycation. AGE-R1 is a scavenger receptor that is responsible for the detoxification and clearance of AGEs, and there is an inverse relationship between AGE-R1 expression and AGE toxicity [26].

Skeletal muscle AGE-R1 expression is lower in diet-induced obese mice, which also show AGE accumulation, higher RAGE expression, and lower of myogenic capacity [32, 33]. These findings suggest that AGE-R1 expression may be lower in unloaded muscles, which may contribute to muscle dysfunction. However, in the present study, we found that AGE-R1 expression was higher in microgravity-induced atrophic muscle and that this change was ameliorated by RAGE inhibition (Figure 4). Because AGE-R1 has been shown to have a counter-regulatory effect on the AGE-RAGE axis [34], the upregulation of AGE-R1 may be a compensatory mechanism to offset activation of the AGE-RAGE axis during microgravity exposure.

In addition to AGE-R1, glyoxalase, aldose reductase, and aldehyde dehydrogenase are considered to participate in the defense against AGEs accumulation [27]. Dysfunction of MG detoxification causes the development of aging-associated diseases, such as diabetes, renal failure, cardiovascular disease, and cancer [35]. Furthermore, a recent study showed that the glyoxalase system is dysregulated in the skeletal muscle of diabetic patients, thereby contributing to muscle insulin resistance [36]. A clinical trial conducted in overweight and obese patients demonstrated that a drug that induces glyoxalase 1 activity reduces the risk of developing diabetes, potentially by reducing RAGE expression [37]. The results of the present study, that glyoxalase 1, aldose reductase, and ALDH2 expression is high during hindlimb suspension (Figure 4), suggest that these enzymes may have been upregulated in response to the increase in MG-derived AGE formation during microgravity exposure, as in AGE-R1.

The inflammatory response, which involves the upregulation of proinflammatory cytokines, such as TNFα, IL-1β, and IL-6, is thought to be involved in skeletal muscle atrophy [38]. High TNFα, IL-1β, and IL-6 levels have been reported to be associated with microgravity-induced muscle atrophy in humans [39] and rodents [40-43], and high expression of TNFα, IL-1β, and IL-6 mRNA was identified in the present study (Figure 5). In this context, it has been reported that the activation of RAGE is closely related to a sustained inflammatory response [44]. A previous study showed that RAGE gene promoter activity correlates with TNFα, IL-1β, and IL-6 production in peripheral blood mononuclear cells from diabetic patients [45]. In addition, a RAGE-neutralizing antibody has been shown to reduce AGE-induced upregulation of IL-1β in mouse macrophages [46]. In the present study, RAGE inhibition ameliorated the increases in TNFα, IL-1β,

and IL-6 expression induced by hindlimb suspension (Figure 5). It has also been previously reported that the inhibition of IL-6 ameliorates hindlimb suspension-induced skeletal muscle atrophy [47]. Therefore, RAGE inhibition may ameliorate skeletal muscle atrophy by reducing the expression of proinflammatory cytokines.

Proinflammatory cytokines are released from macrophages and neutrophils in response to inflammatory stimuli. However, it is controversial that unloading stress recruits macrophages and neutrophils into skeletal muscle. Some studies have shown that the recruitment of macrophages and neutrophils did not occur in soleus muscle after 7 to 10 days hindlimb suspension [48, 49], whereas other study has reported the upregulation of macrophages and neutrophils expressions [50]. In the present study, we did not check the whole inflammatory process, and therefore it needs further studies to clear the involvement of a series of inflammation processes in the RAGE-associated regulation of muscle adaptations during microgravity exposure.

In conclusion, our findings indicate that the AGE-RAGE axis is upregulated in skeletal muscle under microgravity environment, and that RAGE inhibition ameliorates microgravity-induced skeletal muscle atrophy, proinflammatory cytokine expression, and the activation of the ubiquitin-proteasome system. To the best of our knowledge, this is the first study to show the involvement of the AGE-RAGE axis in skeletal muscle atrophy induced by microgravity exposure. The present findings contribute to our understanding of the complex molecular responses that occur during microgravity-associated skeletal muscle adaptation.

References

[1] J.M. Argiles, N. Campos, J.M. Lopez-Pedrosa, R. Rueda, L. Rodriguez-Manas, Skeletal Muscle Regulates Metabolism via Interorgan Crosstalk: Roles in Health and Disease, J Am Med Dir Assoc, 17 (2016) 789-796 https://doi.org/10.1016/j.jamda.2016.04.019.

[2] T. Ohira, F. Kawano, T. Ohira, K. Goto, Y. Ohira, Responses of skeletal muscles to gravitational unloading and/or reloading, J Physiol Sci, 65 (2015) 293-310 https://doi.org/10.1007/s12576-015-0375-6.

[3] C.Y. Chiu, R.S. Yang, M.L. Sheu, D.C. Chan, T.H. Yang, K.S. Tsai, C.K. Chiang, S.H. Liu, Advanced glycation end-products induce skeletal muscle atrophy and dysfunction in diabetic mice via a RAGE-mediated, AMPK-down-regulated, Akt pathway, J. Pathol., 238 (2016) 470-482 https://doi.org/10.1002/path.4674.

[4] F. Riuzzi, G. Sorci, R. Sagheddu, S. Chiappalupi, L. Salvadori, R. Donato, RAGE in the pathophysiology of skeletal muscle, J Cachexia Sarcopenia Muscle, 9 (2018) 1213-1234 https://doi.org/10.1002/jcsm.12350.

[5] M. Fournet, F. Bonte, A. Desmouliere, Glycation Damage: A Possible Hub for Major Pathophysiological Disorders and Aging, Aging Dis, 9 (2018) 880-900 https://doi.org/10.14336/AD.2017.1121.

[6] M. Dalal, L. Ferrucci, K. Sun, J. Beck, L.P. Fried, R.D. Semba, Elevated serum advanced glycation end products and poor grip strength in older community-dwelling women, J. Gerontol. A. Biol. Sci. Med. Sci., 64 (2009) 132-137 https://doi.org/10.1093/gerona/gln018.

[7] R.D. Semba, S. Bandinelli, K. Sun, J.M. Guralnik, L. Ferrucci, Relationship of an advanced glycation end product, plasma carboxymethyl-lysine, with slow walking

speed in older adults: the InCHIANTI study, Eur. J. Appl. Physiol., 108 (2010) 191-195 https://doi.org/10.1007/s00421-009-1192-5.

[8] T. Egawa, Y. Ohno, S. Yokoyama, A. Goto, R. Ito, T. Hayashi, K. Goto, The effect of advanced glycation end products on cellular signaling molecules in skeletal muscle, J. Phys. Fit. Sports Med., 7 (2018) 229-238 https://doi.org/10.7600/jpfsm.7.229.

[9] T. Egawa, S. Tsuda, A. Goto, Y. Ohno, S. Yokoyama, K. Goto, T. Hayashi, Potential involvement of dietary advanced glycation end products in impairment of skeletal muscle growth and muscle contractile function in mice, Br. J. Nutr., 117 (2017) 21-29 https://doi.org/10.1017/S0007114516004591.

[10] K. Asadipooya, E.M. Uy, Advanced Glycation End Products (AGEs), Receptor for AGEs, Diabetes, and Bone: Review of the Literature, J Endocr Soc, 3 (2019) 1799-1818 https://doi.org/10.1210/js.2019-00160.

[11] S. Bongarzone, V. Savickas, F. Luzi, A.D. Gee, Targeting the Receptor for Advanced Glycation Endproducts (RAGE): A Medicinal Chemistry Perspective, J. Med. Chem., 60 (2017) 7213-7232 https://doi.org/10.1021/acs.jmedchem.7b00058.

[12] B.I. Hudson, M.E. Lippman, Targeting RAGE Signaling in Inflammatory Disease, Annu. Rev. Med., 69 (2018) 349-364 https://doi.org/10.1146/annurev-med-041316-085215.

[13] A.H. Burstein, I. Grimes, D.R. Galasko, P.S. Aisen, M. Sabbagh, A.M. Mjalli, Effect of TTP488 in patients with mild to moderate Alzheimer's disease, BMC Neurol, 14 (2014) 12 https://doi.org/10.1186/1471-2377-14-12.

[14] R. Deane, I. Singh, A.P. Sagare, R.D. Bell, N.T. Ross, B. LaRue, R. Love, S. Perry, N. Paquette, R.J. Deane, M. Thiyagarajan, T. Zarcone, G. Fritz, A.E. Friedman, B.L. Miller, B.V. Zlokovic, A multimodal RAGE-specific inhibitor reduces amyloid beta-

mediated brain disorder in a mouse model of Alzheimer disease, J. Clin. Invest., 122 (2012) 1377-1392 https://doi.org/10.1172/JCI58642.

[15] A. Cassese, I. Esposito, F. Fiory, A.P. Barbagallo, F. Paturzo, P. Mirra, L. Ulianich, F. Giacco, C. Iadicicco, A. Lombardi, F. Oriente, E. Van Obberghen, F. Beguinot, P. Formisano, C. Miele, In skeletal muscle advanced glycation end products (AGEs) inhibit insulin action and induce the formation of multimolecular complexes including the receptor for AGEs, J. Biol. Chem., 283 (2008) 36088-36099 https://doi.org/10.1074/jbc.M801698200.

[16] H.M. Davis, A.L. Essex, S. Valdez, P.J. Deosthale, M.W. Aref, M.R. Allen, A. Bonetto, L.I. Plotkin, Short-term pharmacologic RAGE inhibition differentially affects bone and skeletal muscle in middle-aged mice, Bone, 124 (2019) 89-102 https://doi.org/10.1016/j.bone.2019.04.012.

[17] T. Egawa, A. Goto, Y. Ohno, S. Yokoyama, A. Ikuta, M. Suzuki, T. Sugiura, Y. Ohira, T. Yoshioka, T. Hayashi, K. Goto, Involvement of AMPK in regulating slow-twitch muscle atrophy during hindlimb unloading in mice, Am J Physiol Endocrinol Metab, 309 (2015) E651-662 https://doi.org/10.1152/ajpendo.00165.2015.

[18] I. Sharma, R.S. Tupe, A.K. Wallner, Y.S. Kanwar, Contribution of myo-inositol oxygenase in AGE:RAGE-mediated renal tubulointerstitial injury in the context of diabetic nephropathy, Am J Physiol Renal Physiol, 314 (2018) F107-F121 https://doi.org/10.1152/ajprenal.00434.2017.

[19] T. Egawa, S. Tsuda, X. Ma, T. Hamada, T. Hayashi, Caffeine modulates phosphorylation of insulin receptor substrate-1 and impairs insulin signal transduction in rat skeletal muscle, J Appl Physiol (1985), 111 (2011) 1629-1636 https://doi.org/10.1152/japplphysiol.00249.2011.

[20] Y. Ohno, S. Yamada, T. Sugiura, Y. Ohira, T. Yoshioka, K. Goto, A possible role of NF-kappaB and HSP72 in skeletal muscle hypertrophy induced by heat stress in rats, Gen. Physiol. Biophys., 29 (2010) 234-242 https://doi.org/10.4149/gpb_2010_03_234.

[21] D. Hawkins, C. Karlsson, M. Gammell, Statistical power, effect size and animal welfare: recommendations for good practice, 22 (2013) 339-344 https://doi.org/10.7120/09627286.22.3.339.

[22] A. Schmitt, J. Schmitt, G. Munch, J. Gasic-Milencovic, Characterization of advanced glycation end products for biochemical studies: side chain modifications and fluorescence characteristics, Anal. Biochem., 338 (2005) 201-215 https://doi.org/10.1016/j.ab.2004.12.003.

[23] S. Ciciliot, A.C. Rossi, K.A. Dyar, B. Blaauw, S. Schiaffino, Muscle type and fiber type specificity in muscle wasting, Int. J. Biochem. Cell Biol., 45 (2013) 2191-2199 https://doi.org/10.1016/j.biocel.2013.05.016.

[24] T. Kislinger, C. Fu, B. Huber, W. Qu, A. Taguchi, S. Du Yan, M. Hofmann, S.F. Yan, M. Pischetsrieder, D. Stern, A.M. Schmidt, N(epsilon)-(carboxymethyl)lysine adducts of proteins are ligands for receptor for advanced glycation end products that activate cell signaling pathways and modulate gene expression, J. Biol. Chem., 274 (1999) 31740-31749 https://doi.org/10.1074/jbc.274.44.31740.

[25] J. Xue, R. Ray, D. Singer, D. Bohme, D.S. Burz, V. Rai, R. Hoffmann, A. Shekhtman, The receptor for advanced glycation end products (RAGE) specifically recognizes methylglyoxal-derived AGEs, Biochemistry (Mosc). 53 (2014) 3327-3335 https://doi.org/10.1021/bi500046t.

[26] C. Ott, K. Jacobs, E. Haucke, A. Navarrete Santos, T. Grune, A. Simm, Role of

advanced glycation end products in cellular signaling, Redox Biol, 2 (2014) 411-429 https://doi.org/10.1016/j.redox.2013.12.016.

[27] D.L. Vander Jagt, L.A. Hunsaker, Methylglyoxal metabolism and diabetic complications: roles of aldose reductase, glyoxalase-I, betaine aldehyde dehydrogenase and 2-oxoaldehyde dehydrogenase, Chem. Biol. Interact., 143-144 (2003) 341-351 https://doi.org/10.1016/s0009-2797(02)00212-0.

[28] G. Lopez-Castejon, D. Brough, Understanding the mechanism of IL-1beta secretion, Cytokine Growth Factor Rev., 22 (2011) 189-195 https://doi.org/10.1016/j.cytogfr.2011.10.001.

[29] R.D. Semba, E.J. Nicklett, L. Ferrucci, Does accumulation of advanced glycation end products contribute to the aging phenotype?, J. Gerontol. A. Biol. Sci. Med. Sci., 65 (2010) 963-975 https://doi.org/10.1093/gerona/glq074.

[30] L.M. Snow, N.A. Fugere, L.V. Thompson, Advanced glycation end-product accumulation and associated protein modification in type II skeletal muscle with aging, J. Gerontol. A. Biol. Sci. Med. Sci., 62 (2007) 1204-1210 https://doi.org/10.1093/gerona/62.11.1204.

[31] B. Ramamurthy, L. Larsson, Detection of an aging-related increase in advanced glycation end products in fast- and slow-twitch skeletal muscles in the rat, Biogerontology, 14 (2013) 293-301 https://doi.org/10.1007/s10522-013-9430-y.

[32] R. Mastrocola, M. Collino, D. Nigro, F. Chiazza, G. D'Antona, M. Aragno, M.A. Minetto, Accumulation of advanced glycation end-products and activation of the SCAP/SREBP Lipogenetic pathway occur in diet-induced obese mouse skeletal muscle, PLoS One, 10 (2015) e0119587 https://doi.org/10.1371/journal.pone.0119587.

[33] R. Mastrocola, D. Nigro, F. Chiazza, C. Medana, F. Dal Bello, G. Boccuzzi, M. Collino, M. Aragno, Fructose-derived advanced glycation end-products drive lipogenesis and skeletal muscle reprogramming via SREBP-1c dysregulation in mice, Free Radic. Biol. Med., 91 (2016) 224-235 https://doi.org/10.1016/j.freeradbiomed.2015.12.022.

[34] C. Lu, J.C. He, W. Cai, H. Liu, L. Zhu, H. Vlassara, Advanced glycation endproduct (AGE) receptor 1 is a negative regulator of the inflammatory response to AGE in mesangial cells, Proc. Natl. Acad. Sci. U. S. A., 101 (2004) 11767-11772 https://doi.org/10.1073/pnas.0401588101.

[35] N. Rabbani, M. Xue, P.J. Thornalley, Methylglyoxal-induced dicarbonyl stress in aging and disease: first steps towards glyoxalase 1-based treatments, Clin Sci (Lond), 130 (2016) 1677-1696 https://doi.org/10.1042/CS20160025.

[36] J.T. Mey, B.K. Blackburn, E.R. Miranda, A.B. Chaves, J. Briller, M.G. Bonini, J.M. Haus, Dicarbonyl stress and glyoxalase enzyme system regulation in human skeletal muscle, Am J Physiol Regul Integr Comp Physiol, 314 (2018) R181-R190 https://doi.org/10.1152/ajpregu.00159.2017.

[37] M. Xue, M.O. Weickert, S. Qureshi, N.B. Kandala, A. Anwar, M. Waldron, A. Shafie, D. Messenger, M. Fowler, G. Jenkins, N. Rabbani, P.J. Thornalley, Improved Glycemic Control and Vascular Function in Overweight and Obese Subjects by Glyoxalase 1 Inducer Formulation, Diabetes, 65 (2016) 2282-2294 https://doi.org/10.2337/db16-0153.

[38] P. Londhe, D.C. Guttridge, Inflammation induced loss of skeletal muscle, Bone, 80 (2015) 131-142 https://doi.org/10.1016/j.bone.2015.03.015.

[39] L. Breen, K.A. Stokes, T.A. Churchward-Venne, D.R. Moore, S.K. Baker, K. Smith,

P.J. Atherton, S.M. Phillips, Two weeks of reduced activity decreases leg lean mass and induces "anabolic resistance" of myofibrillar protein synthesis in healthy elderly, J. Clin. Endocrinol. Metab., 98 (2013) 2604-2612 https://doi.org/10.1210/jc.2013-1502.

[40] T. Hirose, K. Nakazato, H. Song, N. Ishii, TGF-beta1 and TNF-alpha are involved in the transcription of type I collagen alpha2 gene in soleus muscle atrophied by mechanical unloading, J Appl Physiol (1985), 104 (2008) 170-177 https://doi.org/10.1152/japplphysiol.00463.2006.

[41] S. Al-Nassan, N. Fujita, H. Kondo, S. Murakami, H. Fujino, Chronic Exercise Training Down-Regulates TNF-alpha and Atrogin-1/MAFbx in Mouse Gastrocnemius Muscle Atrophy Induced by Hindlimb Unloading, Acta Histochem Cytochem, 45 (2012) 343-349 https://doi.org/10.1267/ahc.12023.

[42] S.M. Lang, A.A. Kazi, L. Hong-Brown, C.H. Lang, Delayed recovery of skeletal muscle mass following hindlimb immobilization in mTOR heterozygous mice, PLoS One, 7 (2012) e38910 https://doi.org/10.1371/journal.pone.0038910.

[43] C. Kang, C.A. Goodman, T.A. Hornberger, L.L. Ji, PGC-1alpha overexpression by in vivo transfection attenuates mitochondrial deterioration of skeletal muscle caused by immobilization, FASEB J., 29 (2015) 4092-4106 https://doi.org/10.1096/fj.14-266619.

[44] K. Kierdorf, G. Fritz, RAGE regulation and signaling in inflammation and beyond, J. Leukoc. Biol., 94 (2013) 55-68 https://doi.org/10.1189/jlb.1012519.

[45] S. Kan, J. Wu, C. Sun, J. Hao, Z. Wu, Correlation between RAGE gene promoter methylation and diabetic retinal inflammation, Exp Ther Med, 15 (2018) 242-246 https://doi.org/10.3892/etm.2017.5378.

[46] Z. Zhou, Y. Tang, X. Jin, C. Chen, Y. Lu, L. Liu, C. Shen, Metformin Inhibits Advanced Glycation End Products-Induced Inflammatory Response in Murine Macrophages Partly through AMPK Activation and RAGE/NFkappaB Pathway Suppression, J Diabetes Res, 2016 (2016) 4847812 https://doi.org/10.1155/2016/4847812.

[47] M. Yakabe, S. Ogawa, H. Ota, K. Iijima, M. Eto, Y. Ouchi, M. Akishita, Inhibition of interleukin-6 decreases atrogene expression and ameliorates tail suspension-induced skeletal muscle atrophy, PLoS One, 13 (2018) e0191318 https://doi.org/10.1371/journal.pone.0191318.

[48] J.M. McClung, J.M. Davis, J.A. Carson, Ovarian hormone status and skeletal muscle inflammation during recovery from disuse in rats, Exp. Physiol., 92 (2007) 219-232 https://doi.org/10.1113/expphysiol.2006.035071.

[49] S. Kohno, Y. Yamashita, T. Abe, K. Hirasaka, M. Oarada, A. Ohno, S. Teshima-Kondo, A. Higashibata, I. Choi, E.M. Mills, Y. Okumura, J. Terao, T. Nikawa, Unloading stress disturbs muscle regeneration through perturbed recruitment and function of macrophages, J Appl Physiol (1985), 112 (2012) 1773-1782 https://doi.org/10.1152/japplphysiol.00103.2012.

[50] H.X. Nguyen, J.G. Tidball, Expression of a muscle-specific, nitric oxide synthase transgene prevents muscle membrane injury and reduces muscle inflammation during modified muscle use in mice, J Physiol, 550 (2003) 347-356 https://doi.org/10.1113/jphysiol.2003.040907.

Conflicts of Interest

The authors declare no conflict of interest.

Acknowledgements

This study was supported in part by JSPS KAKENHI (Tatsuro Egawa, 18H03148 and 19K22806; Kohei Kido, 18J01392 and 19K20007; Takumi Yokokawa, 16J10577; Katsumasa Goto, 18H03160, 19K22825, and 19KK0254; Tatsuya Hayashi, 19K11520). Additional research grants were provided by the Science Research Promotion Fund from the Promotion and Mutual Aid Corporation for Private Schools of Japan; and Graduate School of Health Sciences, Toyohashi SOZO University (KG).

Figure Legends

Figure 1

The fluorescence intensity of advanced glycation end-products (AGEs) (A) and receptor for AGEs (RAGE) expression (B) in soleus, plantaris, and extensor digitorum longus (EDL) muscle after hindlimb suspension. Mice in the HS group were subjected to continuous hindlimb suspension for 1 week. Age-matched mice that did not undergo hindlimb suspension were used as controls (CON). The fluorescence intensity associated with AGEs were measured using 360 nm excitation and 460 nm emission wavelengths. The intensity levels are expressed in arbitrary units. Data are means ± SE; n=6–8 per group. Individual data points are indicated on the bar graph. Representative images of immunoblots and CBB staining are shown. The value of effect size is listed in parentheses.

Figure 2

Soleus mass normalized to body mass (A), muscle fiber cross sectional area (CSA) (B), and myosin heavy chain (MyHC) slow-type expression (C) after hindlimb suspension and/or RAGE antagonist treatment. Mice in the HS group were subjected to continuous hindlimb suspension for 1 week. Age-matched mice that did not undergo hindlimb suspension were used as controls (CON). Mice in the HS + FPS-ZM1 group were injected daily intraperitoneally with 1 mg/kg FPS-ZM1, a RAGE antagonist, during hindlimb suspension. Data are means ± SE; n=7–9 per group. Individual data points are indicated on the bar graph. Representative images of immunofluorescence, immunoblots, and CBB staining are shown. Scale bars, 50 μm. The value of effect size is listed in parentheses.

Figure 3

The level of methylglyoxal (MG)-modified proteins and Nε-(carboxymethyl) lysine (CML)-modified proteins after hindlimb suspension and/or RAGE antagonist treatment (A), and the interaction between MG- or CML-modified protein level and muscle mass (B). For the quantification of MG-modified proteins and CML-modified proteins, the signal intensity of full-molecular-weight were quantified. Data are means ± SE; n=8 per group. Individual data points are indicated on the bar graph. Representative images of immunoblots and CBB staining are shown. The value of effect size is listed in parentheses.

Figure 4

The expression of AGE receptor 1 (AGE-R1), glyoxalase 1, aldose reductase, and aldehyde dehydrogenase (ALDH) 2 after hindlimb suspension and/or RAGE antagonist treatment. Data are means ± SE; n=8 per group. Individual data points are indicated on the bar graph. Representative images of immunoblots and CBB staining are shown. The value of effect size is listed in parentheses.

Figure 5

The expression of tumor necrosis factor (TNF) α, interleukin (IL)-1β, and IL-6 after hindlimb suspension and/or RAGE antagonist treatment. Data are means ± SE; n=8 per group. Individual data points are indicated on the bar graph. Representative images of immunoblots and CBB staining are shown. The value of effect size is listed in parentheses.

Figure 6

The expression of *Trim63*, *Fbox32*, and *Wwp1* mRNA (A), and muscle-specific RING finger 1 (MuRF1) protein and K48-ubiquitinated proteins (K48-Ub) (B) after hindlimb suspension and/or RAGE antagonist treatment. For the quantification of K48-ubiquitinated proteins, the signal intensity of full-molecular-weight were quantified. Data are means ± SE; n=7–8 per group. Individual data points are indicated on the bar graph. Representative images of immunoblots and CBB staining are shown. The value of effect size is listed in parentheses.

Figure 7

The phosphorylation level of Unc-51-like kinase 1 (Ulk1) Ser^{757}, the microtubule-associated protein 1 light chain 3 (LC3) II/LC3I ratio, p62 expression, and the phosphorylation level of 70-kDa ribosomal S6 kinase (p70S6K) Thr^{389} after hindlimb suspension and/or RAGE antagonist treatment. Data are means ± SE; n=6–8 per group. Individual data points are indicated on the bar graph. Representative images of immunoblots and CBB staining are shown. The value of effect size is listed in parentheses.

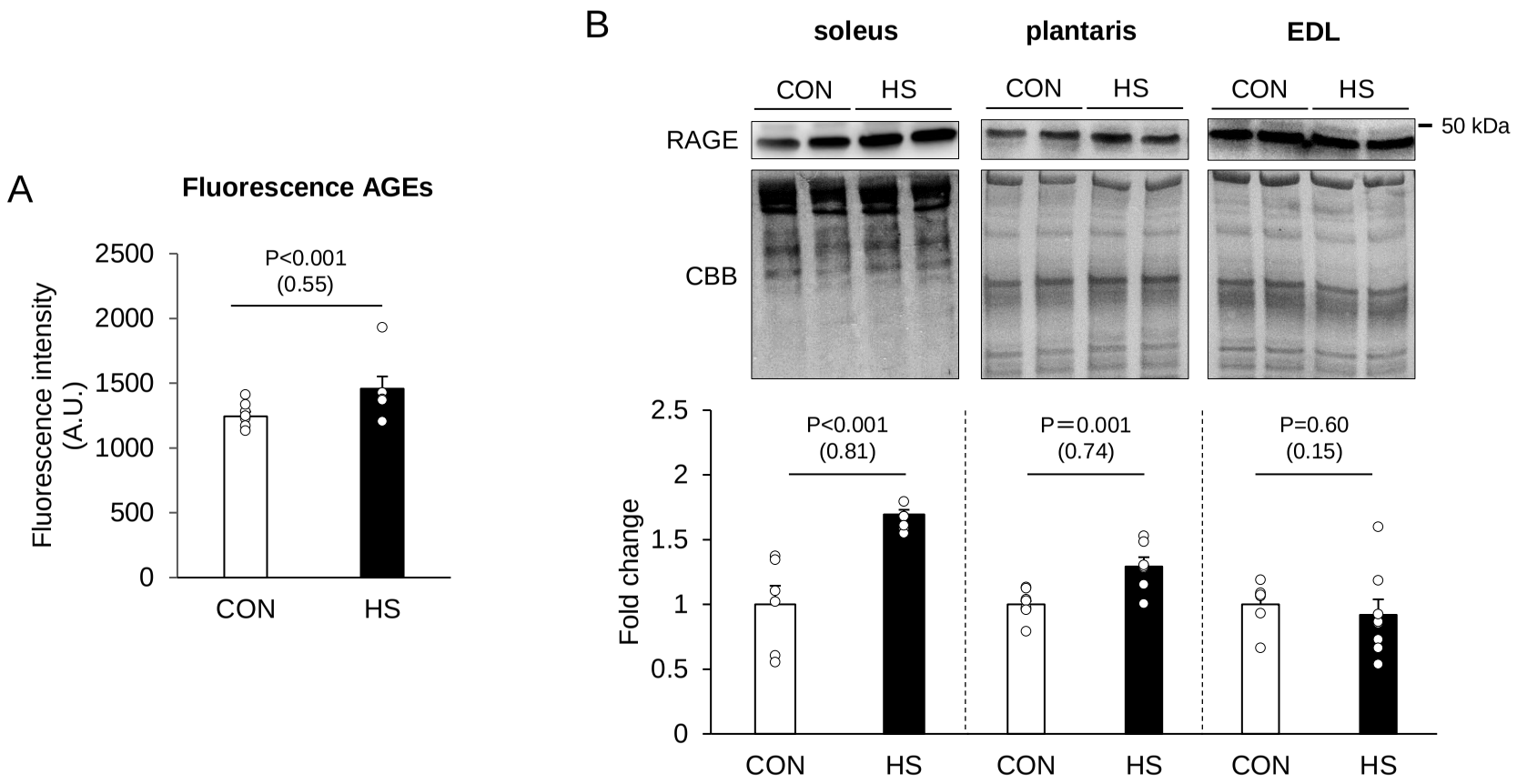
A
Fluorescence AGEs
Fluorescence intensity (A.U.)
2500
2000
1500
1000
500
0
P<0.001
(0.55)
CON
HS
B
soleus
plantaris
EDL
CON
HS
CON
HS
CON
HS
RAGE
50 kDa
CBB
Fold change
2.5
2
1.5
1
0.5
0
P<0.001
(0.81)
P=0.001
(0.74)
P=0.60
(0.15)
CON
HS
CON
HS
CON
HS

Figure 1

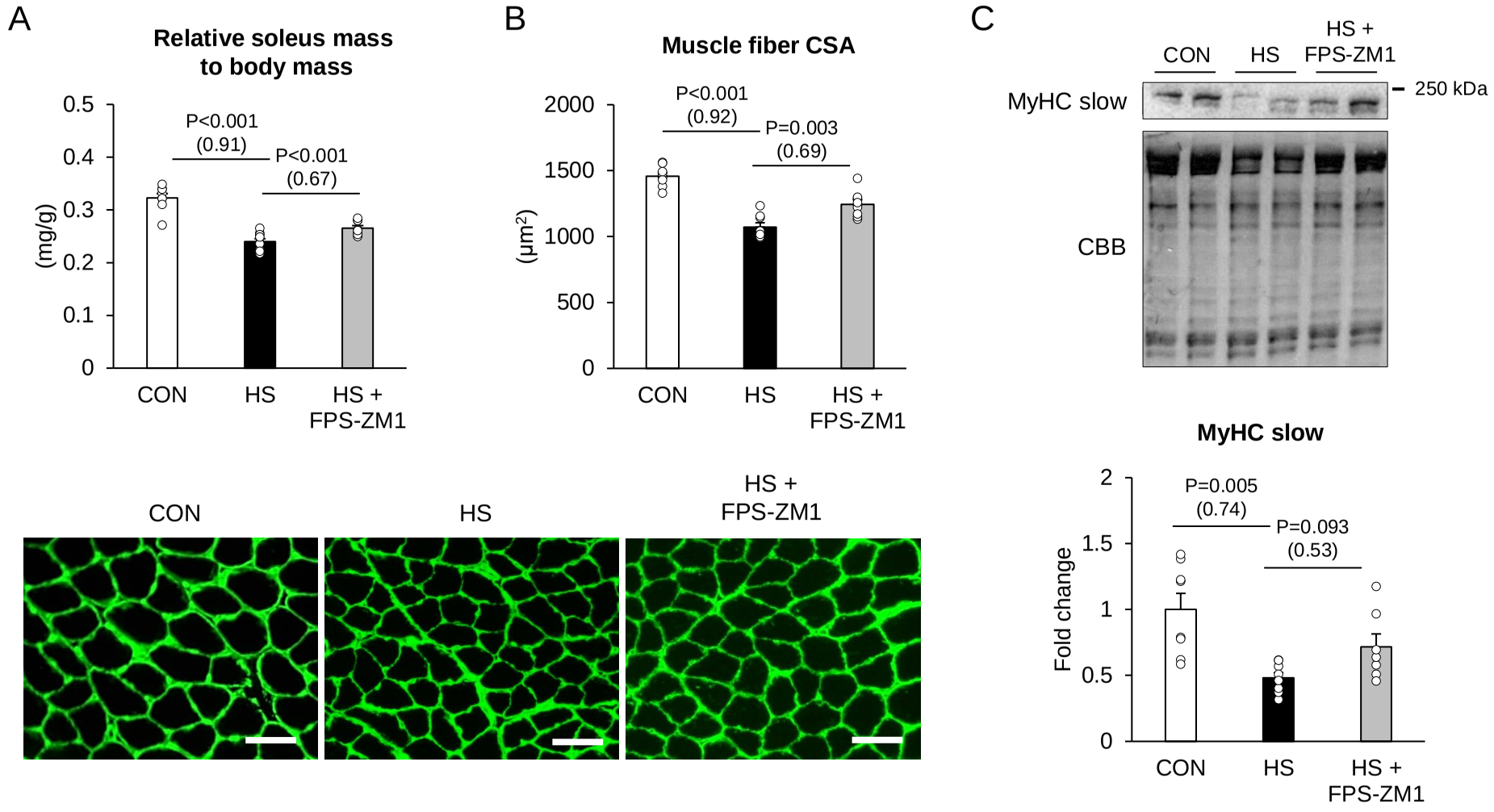
A
Relative soleus mass to body mass
(mg/g)
0.5
0.4
0.3
0.2
0.1
0
P<0.001 (0.91)
P<0.001 (0.67)
CON
HS
HS + FPS-ZM1
B
Muscle fiber CSA
(μm²)
2000
1500
1000
500
0
P<0.001 (0.92)
P=0.003 (0.69)
CON
HS
HS + FPS-ZM1
C
CON
HS
HS + FPS-ZM1
MyHC slow
250 kDa
CBB
MyHC slow
Fold change
2
1.5
1
0.5
0
P=0.005 (0.74)
P=0.093 (0.53)
CON
HS
HS + FPS-ZM1
CON
HS
HS + FPS-ZM1

Figure 2

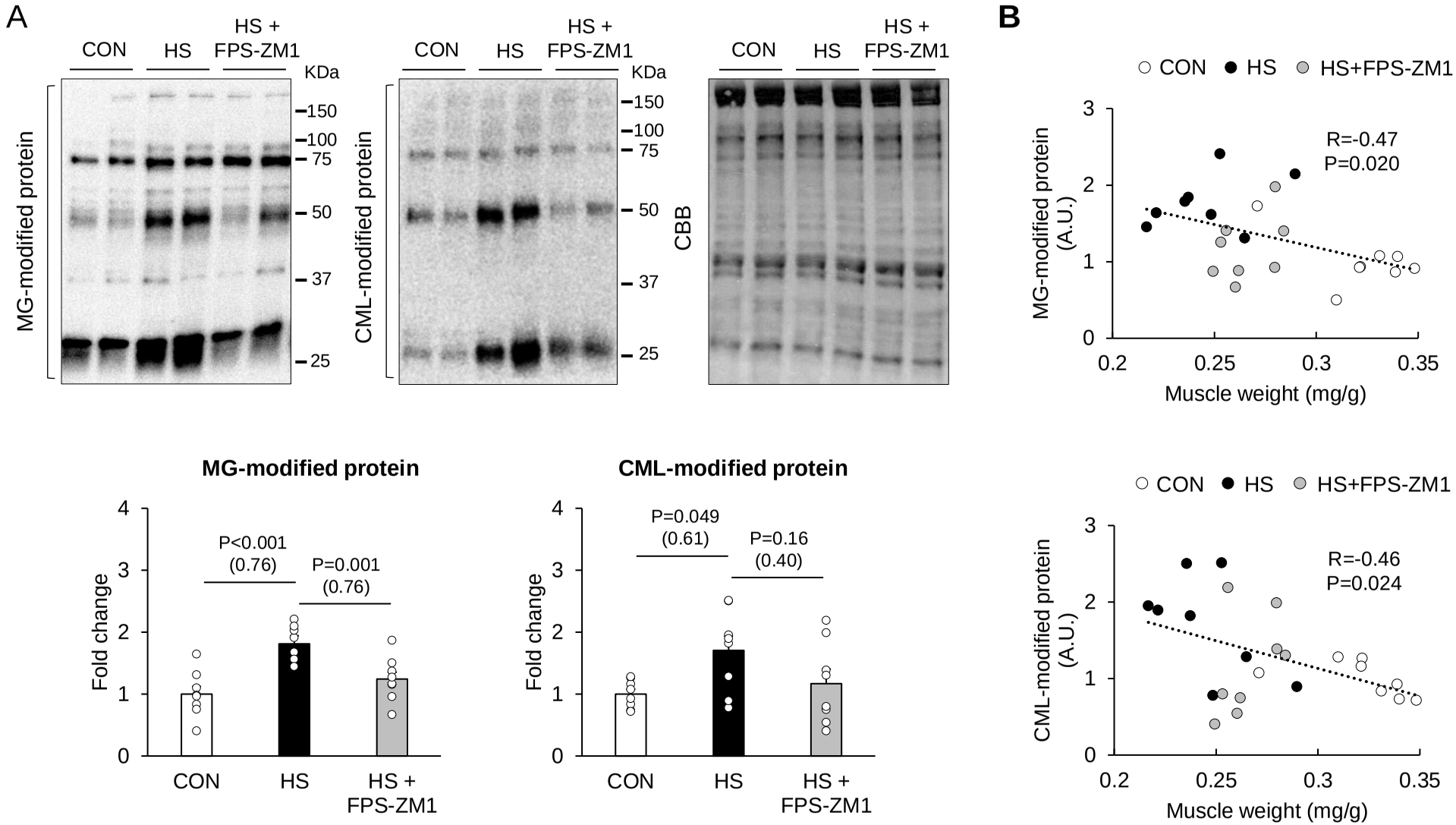
A
CON
HS
HS + FPS-ZM1
KDa
150
100
75
50
37
25
MG-modified protein
CML-modified protein
CBB
MG-modified protein
CML-modified protein
Fold change
P<0.001 (0.76)
P=0.001 (0.76)
P=0.049 (0.61)
P=0.16 (0.40)
B
CON
HS
HS+FPS-ZM1
MG-modified protein (A.U.)
R=-0.47
P=0.020
CML-modified protein (A.U.)
R=-0.46
P=0.024
Muscle weight (mg/g)

Figure 3

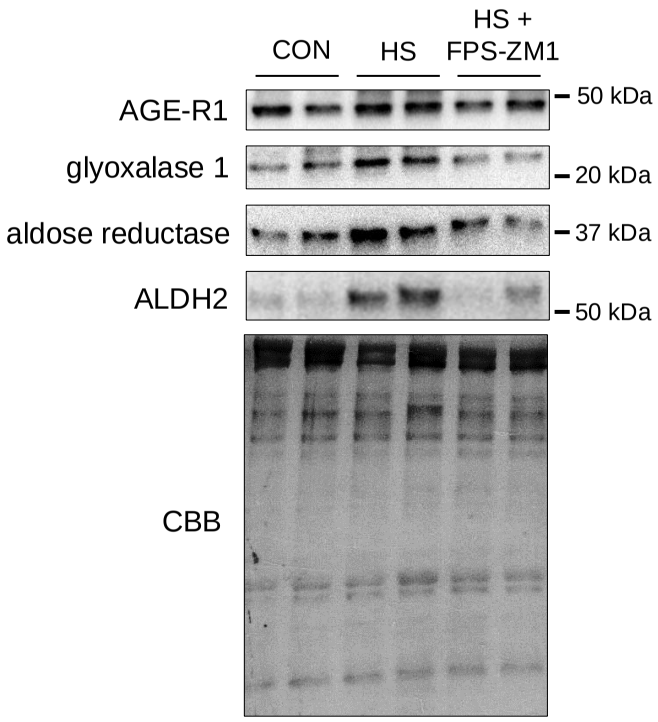
CON
HS
HS +
FPS-ZM1
AGE-R1
glyoxalase 1
aldose reductase
ALDH2
CBB
50 kDa
20 kDa
37 kDa
50 kDa

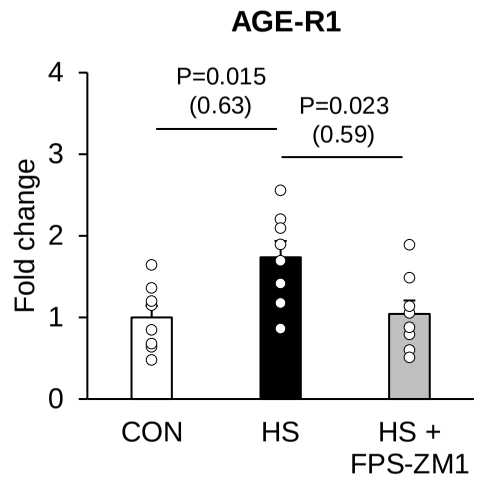
AGE-R1
P=0.015
(0.63)
P=0.023
(0.59)
Fold change
0
1
2
3
4
CON
HS
HS +
FPS-ZM1

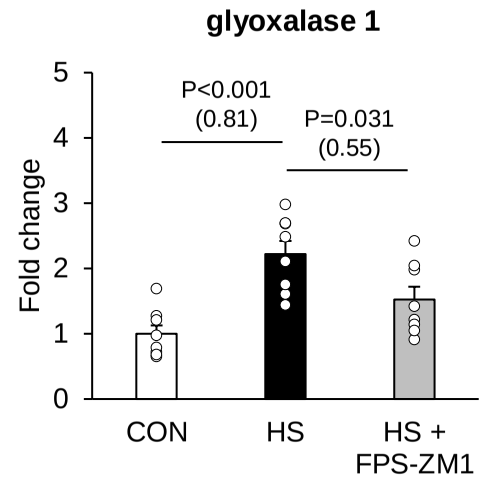
glyoxalase 1
P<0.001
(0.81)
P=0.031
(0.55)
Fold change
0
1
2
3
4
5
CON
HS
HS +
FPS-ZM1

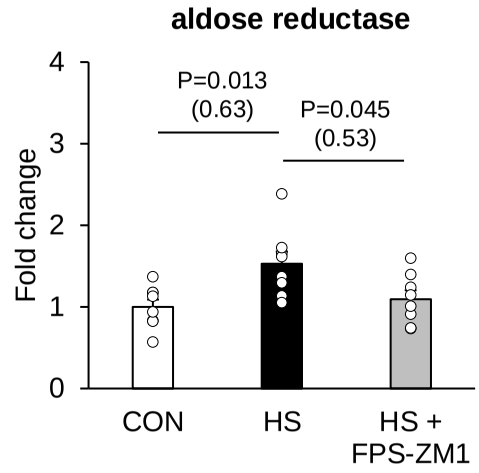
aldose reductase
P=0.013
(0.63)
P=0.045
(0.53)
Fold change
0
1
2
3
4
CON
HS
HS +
FPS-ZM1

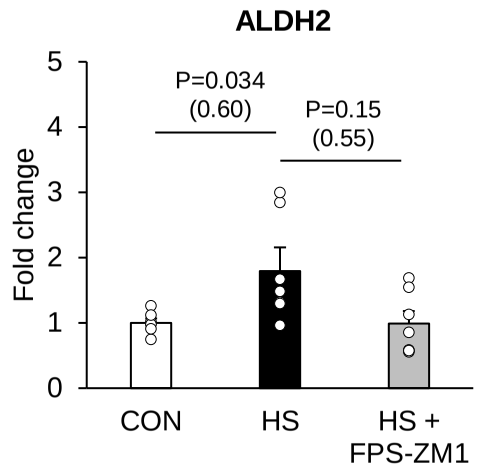
ALDH2
P=0.034
(0.60)
P=0.15
(0.55)
Fold change
0
1
2
3
4
5
CON
HS
HS +
FPS-ZM1

Figure 4

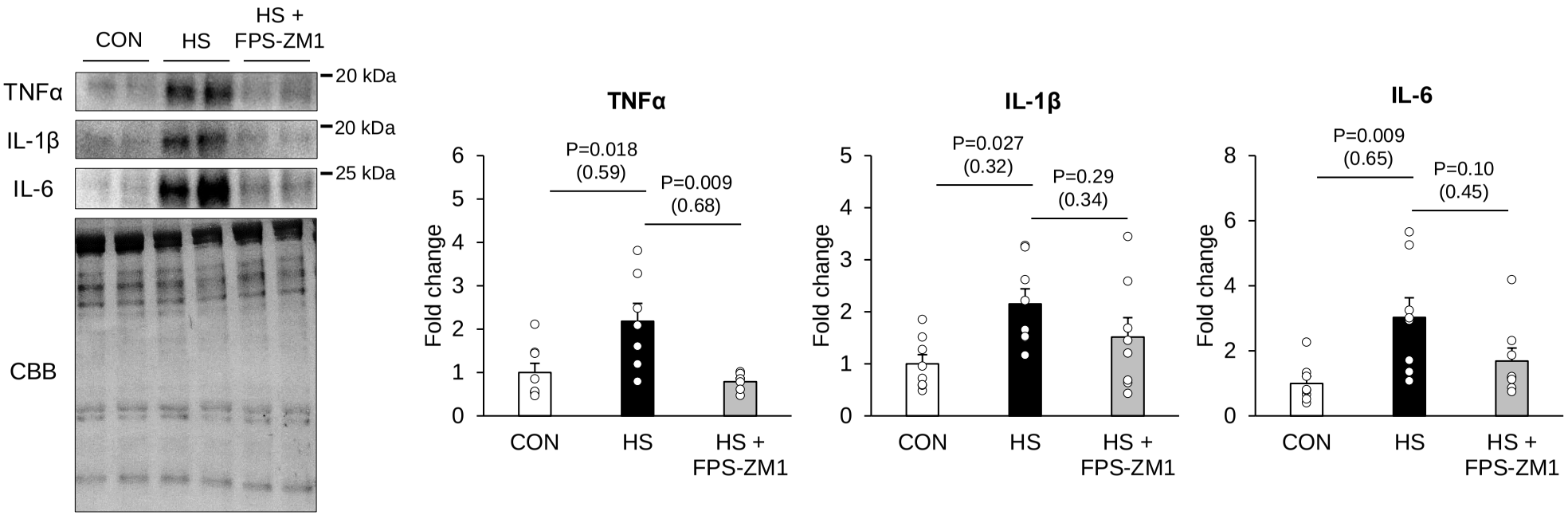
CON
HS
HS +
FPS-ZM1
TNFα
IL-1β
IL-6
CBB
20 kDa
20 kDa
25 kDa
TNFα
IL-1β
IL-6
Fold change
P=0.018
(0.59)
P=0.009
(0.68)
P=0.027
(0.32)
P=0.29
(0.34)
P=0.009
(0.65)
P=0.10
(0.45)
CON
HS
HS +
FPS-ZM1

Figure 5

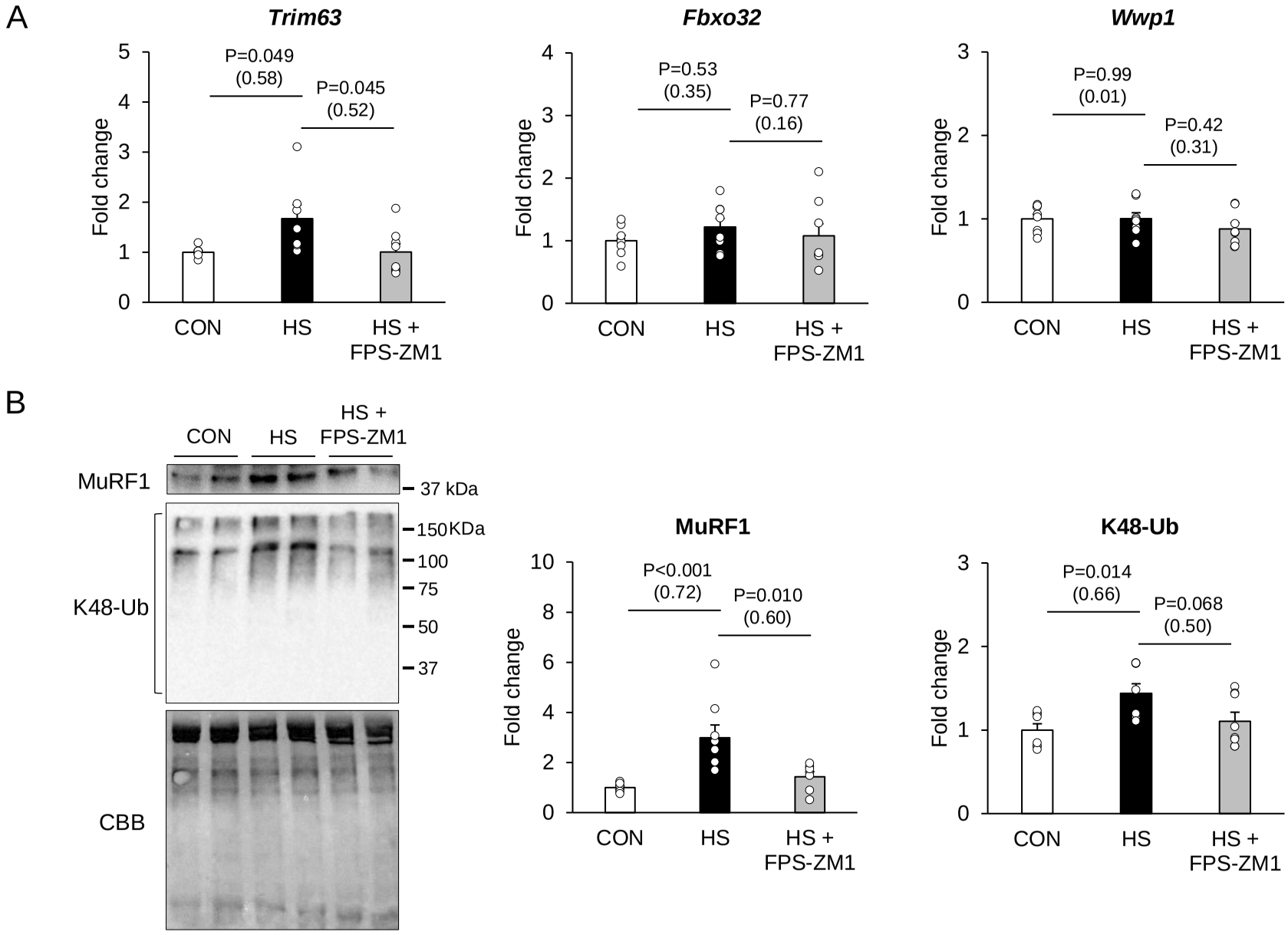
A
Trim63
Fold change
P=0.049
(0.58)
P=0.045
(0.52)
CON
HS
HS +
FPS-ZM1
Fbxo32
P=0.53
(0.35)
P=0.77
(0.16)
Wwp1
P=0.99
(0.01)
P=0.42
(0.31)
B
CON
HS
HS +
FPS-ZM1
MuRF1
37 kDa
K48-Ub
150KDa
100
75
50
37
CBB
MuRF1
P<0.001
(0.72)
P=0.010
(0.60)
K48-Ub
P=0.014
(0.66)
P=0.068
(0.50)

Figure 6

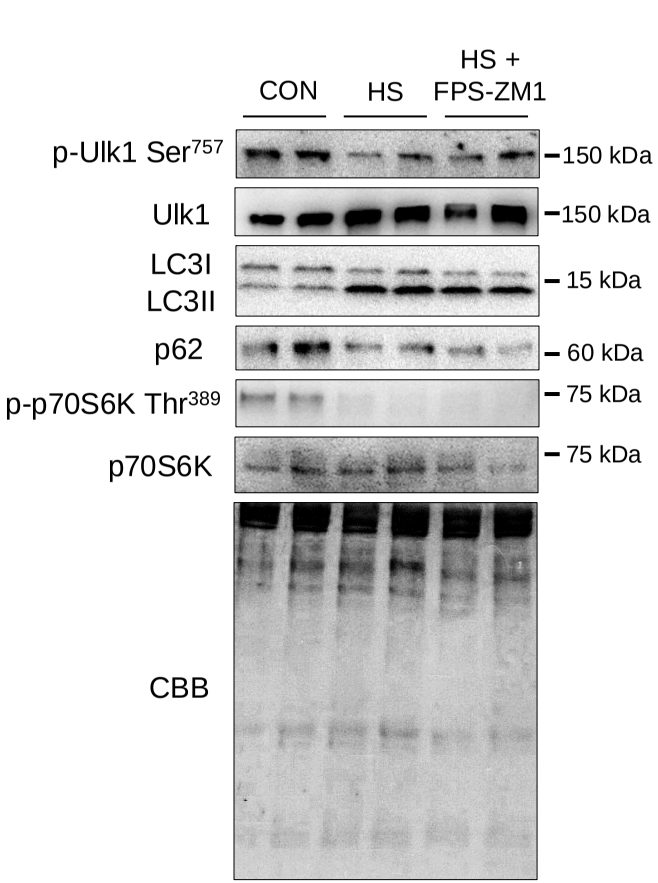
CON
HS
HS +
FPS-ZM1
p-Ulk1 Ser757
Ulk1
LC3I
LC3II
p62
p-p70S6K Thr389
p70S6K
CBB
150 kDa
150 kDa
15 kDa
60 kDa
75 kDa
75 kDa

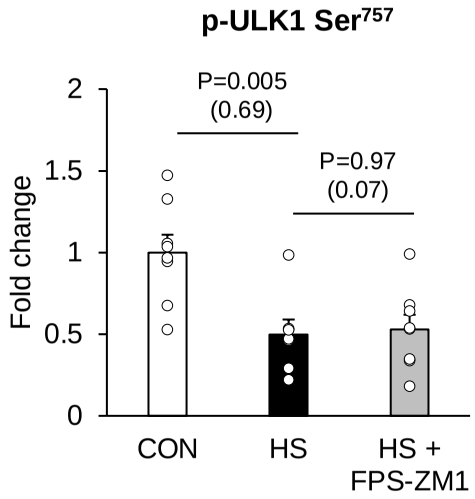
p-ULK1 Ser757
Fold change
P=0.005
(0.69)
P=0.97
(0.07)
CON
HS
HS +
FPS-ZM1

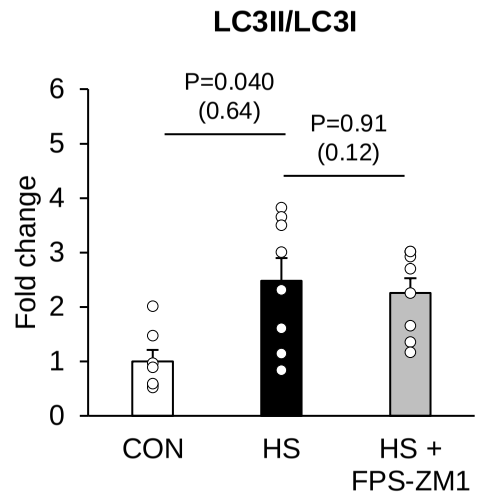
LC3II/LC3I
Fold change
P=0.040
(0.64)
P=0.91
(0.12)
CON
HS
HS +
FPS-ZM1

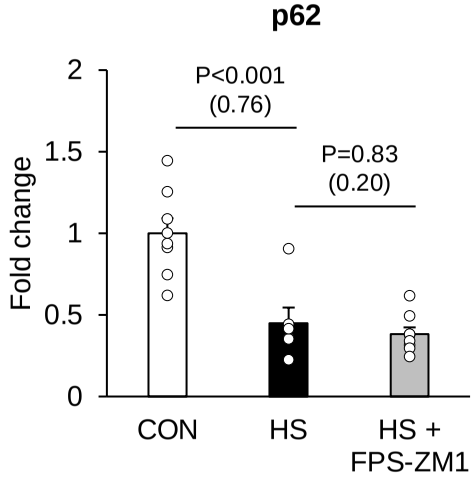
p62
Fold change
P<0.001
(0.76)
P=0.83
(0.20)
CON
HS
HS +
FPS-ZM1

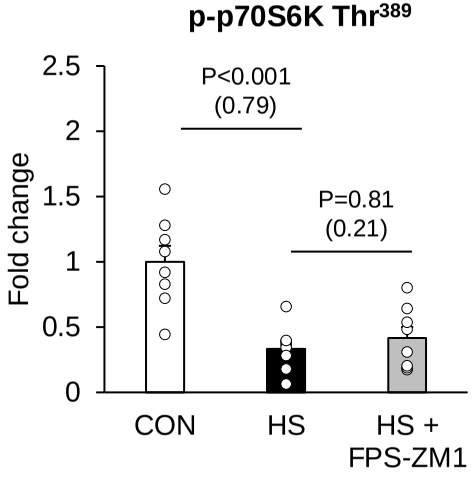
p-p70S6K Thr389
Fold change
P<0.001
(0.79)
P=0.81
(0.21)
CON
HS
HS +
FPS-ZM1

Figure 7